



ELSEVIER

Available online at www.sciencedirect.com

 ScienceDirect

Proceedings of the Combustion Institute 31 (2007) 2001–2009

Proceedings
of the
Combustion
Institute

www.elsevier.com/locate/proci

Combustion of bimodal nano/micron-sized aluminum particle dust in air

Ying Huang, Grant A. Risha, Vigor Yang^{*}, Richard A. Yetter

The Pennsylvania State University, 235 Research Building East, University Park, PA 16802, USA

Abstract

The combustion of bimodal nano/micron-sized aluminum particles with air is studied both analytically and experimentally in a well-characterized laminar particle-laden flow. Experimentally, an apparatus capable of producing Bunsen-type premixed flames was constructed to investigate the flame characteristics of bimodal-particle/air mixtures. The flame speed is positively affected by increasing the mass fraction of nano particles in the fuel formulation despite the lower flame luminosity and thicker flame zone. Theoretically, the flames are assumed to consist of several different regimes for fuel-lean mixture, including the preheat, flame, and post flame zones. The flame speed and temperature distribution are derived by solving the energy equation in each regime and matching the temperature and heat flux at the interfacial boundaries. The analysis allows for the investigation of the effects of particle composition and equivalence ratio on the burning characteristics of aluminum-particle/air mixtures. Reasonable agreement between theoretical results and experimental data was obtained in terms of flame speed. The flame structure of a bimodal particle dust cloud may display either an overlapping or a separated configuration, depending on the combustion properties of aluminum particles at different scales. At low percentages of nano particles in the fuel formulation, the flame exhibits a separated spatial structure with a wider flame regime. At higher nano-particle loadings, overlapping flame configurations are observed.

© 2006 The Combustion Institute. Published by Elsevier Inc. All rights reserved.

Keywords: Nano particle; Micron-sized particle; Metal particle combustion; Particle-laden flow; Aluminum dust combustion

1. Introduction

Aluminum particles have long been employed as a fuel ingredient in various energetic materials to enhance the energy density and stability characteristics of propulsion systems [1–3]. Most previous works were focused on micron-sized particles [4–7], with very limited efforts devoted to the particle behavior at nano scales [8,9].

Nano-metallic particles feature lower ignition temperature, faster burning rate, and consequently shorter burning time because of their high specific-surface area (high reactivity), compared with micron- or larger-sized particles. For very small nano particles, the surface-to-volume ratio may reach a level that the surface energy may qualitatively change their interior “bulk” properties of the material, such as the melting and boiling temperatures. A recent study based on molecular-dynamics simulations indicated that the melting temperature of an aluminum particle of 1 nm can be as low as 400 K [10], which is about

^{*} Corresponding author. Fax: +1 814 865 3389.
E-mail address: vigor@psu.edu (V. Yang).

500 K lower than the bulk value (933 K). In addition, particle diameter plays a significant role in determining combustion mechanisms through its influence on the characteristic transport (diffusion) time relative to the chemical kinetic time. A large particle at high pressure may burn under diffusion-controlled conditions, whereas a small particle at low pressure may burn under kinetically controlled conditions [11–13].

The studies on combustion of particle-laden flows is critical in the design and optimization of combustors for propulsion systems using particulate aluminum as a primary fuel, and results provide valuable information about particle injection, ignition, flame stabilization, and combustor thermal management. Goroshin et al. [14] conducted measurements of flame propagation of aluminum dust in various oxidizer environments in a vertical Pyrex tube. The particle diameter was around 5.4 μm . The flame propagation speed obtained from these tube experiments might not properly represent the actual burning velocity due to the difficulties in defining the flame shape and particle velocity upstream of the flame. Goroshin et al. [15] later established another experimental apparatus capable of producing Bunsen-type premixed dust flames. The dust mass concentration, β , covered a range from 0.25 to 0.60 kg/m^3 , corresponding to the equivalence ratios, ϕ , of 0.81–1.9. The burning velocity was shown to be a weak function of dust concentration for rich aluminum mixtures, a phenomenon that can be attributed to the weak dependence of particle burning rate on the flame temperature in the diffusive regime. Shoshin and Dreizin [16] developed a lifted-flame aerosol burner (LLFAB) for measuring laminar flame speeds of metal–air aerosols over a wide range of particle mass concentrations of 0.4–1.4 kg/m^3 ($1.3 < \phi < 4.5$). Two different aluminum powder sizes (11 and 20 μm) were examined in their experiments. A decrease in the flame speed at very high mass concentration was observed.

In both the works of Goroshin et al. [14,15] and Shoshin and Dreizin [16], micron-sized particles were used. Risha et al. [17] recently examined the flame characteristics of bimodal nano and micron-sized aluminum particle/air laden flows using a Bunsen-burner type apparatus, similar to the experiment of Goroshin et al. [15]. The particle compositions ranged from 100% micron-sized particles (5–8 μm) to mixtures with 30% nano particles (100 nm) by mass. The overall fuel concentration varied from 0.26 to 0.45 kg/m^3 ($0.81 \leq \phi \leq 1.62$). Tests indicated that an increase in percentage of nano particles within the mixture enhanced its flame speed. The flame thickness of bimodal-particle/air mixtures, however, was much wider than that of a micron-sized particle/air mixture.

Although much useful information has been obtained from the preceding studies, the current

knowledge about the combustion of aluminum dust cloud is far from complete. In particular, the effects of particle size and its distribution on the flame characteristics remain to be explored. In the present work, the combustion of aluminum particles in air is theoretically and experimentally studied in a well-characterized laminar flow. Various parameters, such as particle composition and equivalence ratio, on the burning behavior of bimodal aluminum particles/air mixtures are examined in detail.

2. Experiments and observations

The experimental setup consists of a linear actuator, an aerosol generation assembly (AGS), and an aerosol delivery system, as shown schematically in Fig. 1. Briefly, dry aluminum particles are loaded into a cylindrical cartridge to form a packed bed with a loading density ranging from 21% to 42% (depending upon the fuel composition). The aluminum bed is fed into the particle/air mixing region of the AGS at rates ranging from 13.5 to 30.2 cm/min by a piston. The piston is driven by the linear actuator located at the bottom of the AGS. At these feed rates, the equivalence ratio can be adjusted from 0.81 to 1.62. As the packed bed enters the mixing zone, a high-velocity air flow emerging from an 75- μm thick annular slot impinges on the surface of the aluminum particle bed, removes a thin layer of material, and disperses the aluminum particles into the

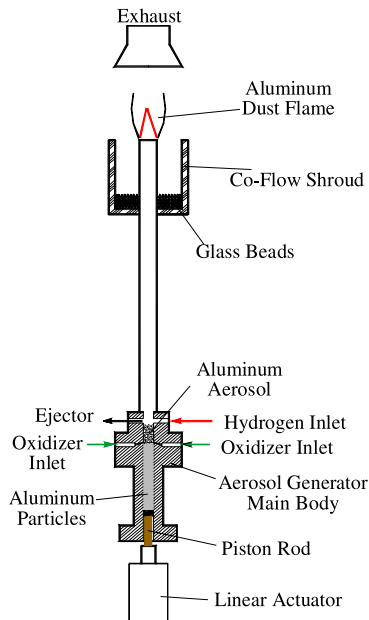


Fig. 1. Schematic diagram of aluminum dust-cloud experimental setup.

incoming air flow to form a homogenous particle laden flow. Immediately above the mixing zone, a high-flow particle ejector was used to divert a portion of the particle-laden flow to bypass the main tube exit. The ejector allows fine tuning of the particle-dust flow rate to stabilize the flame at the nozzle exit. More detailed information about the experimental setup and test conditions can be found in Ref. [17].

Bimodal particle mixtures were formed by mixing nano particles (100 nm) with micron particles (5–8 μm). The particles were dried at 413 K for 24 h before each experiment to improve their dispersion characteristics. The particle-laden flow was ignited by a hydrogen/air pilot flame atop the tube exit. Once steady combustion of the aluminum dust cloud was achieved, the pilot flame was removed. Photographs of the aluminum dust flames were captured by a digital video camera, using three neutral density filters to obtain a clear picture of flame structures. The flame speed was determined based on the total flow rate and measured surface area at the inner edge of the flame zone. Similar to conventional premixed hydrocarbon Bunsen-type flames, our experimental study [17] indicates that the flame can self-adjust by changing its height (surface area) in response to a change in burner flow velocity to maintain a constant laminar flame speed at each equivalence ratio.

Figure 2 shows images of the 100% mono-dispersed micron-sized and bimodal (20% nano-particle addition) aluminum particle dust flames in air. Micron-sized particle mixtures produce a very luminous thin flame zone. Bimodal flames, however, have a thicker reaction zone, which contains two burning regimes (small and larger particles). In addition, flames with nano particles have a smaller cone region with less luminosity, which suggests that nano particles ignite at a lower temperature and burn out quickly. The flame speed is positively affected by the addition of nano parti-

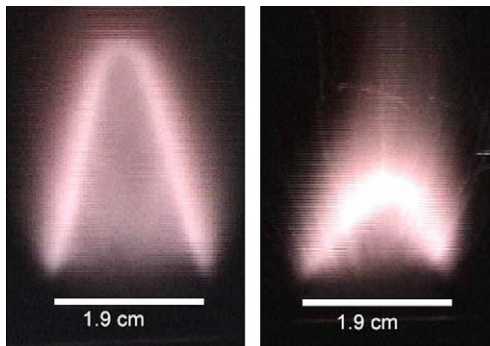


Fig. 2. Images of mono-dispersed (left, 100% micron particles) and bimodal (right, 20% nano particles) aluminum dust flame in air.

cles despite the lower flame luminosity and thicker flame zone. Bimodal mixtures have been successfully stabilized on the burner with mixtures containing up to 30% nano particles by mass. A further increase in the nano-particle mass loading was unsuccessful with the current design of the aerosol generation system.

3. Theoretical analysis

An analytical model was constructed to describe a one-dimensional, freely propagating flame in an aluminum particle-laden flow with a bimodal distribution of particle size. The analysis largely follows the approaches of Goroshin et al. [18], but is extended to include the effect of particle size distribution and variable ignition temperature on the flame behavior. The heat loss of gas to particles is also considered. The major approximations and assumptions are: (1) the dust cloud consists of uniformly distributed aluminum particles at two different sizes with air; (2) the gravitational effects and heat transfer by radiation are neglected; (3) the particle velocity is approximately equal to the gas velocity; (4) collisions and interactions between burning particles are neglected; (5) the Biot number is very small, suggesting a uniform temperature distribution within each particle; (6) the thermal conductivity of the gas, λ , is taken to be constant for simplicity.

The gas-phase governing equations for mass and energy conservation can be written as follows.

$$\rho v = \rho_u S_L \quad (1)$$

$$\rho v C_p dT/dx = \lambda d^2 T/dx^2 + \sum_{i=1}^2 w_{F,i} \cdot Q - \sum_{i=1}^2 n_{p,i} \cdot q_i \quad (2)$$

where ρ , v , and T are the gas density, velocity, and temperature, respectively. The subscripts 1 and 2 denote the properties of small and large powders, respectively, and the subscript u the value related to the unburned mixture. S_L denotes the flame speed, C_p the specific heat of gas at constant pressure, $w_{F,i}$ the mass consumption rate of particle group i , Q the heat of reaction per unit mass of fuel, and $n_{p,i}$ the number density of particle group i (i.e., the number of particles per unit volume). The heat transfer between each particle and surrounding gas, q_i , is given by

$$q_i \approx Nu \cdot 2\pi r_i \lambda (T - T_{s,i}) \quad (3)$$

where the Nusselt number is taken as a constant equal to 2 [19], and T_s is the particle temperature. The equation of state for an isobaric system is

$$\rho T = \text{constant} \quad (4)$$

The energy conservation equation for the particle phase is

$$(\rho_{s,i} v C_s) dT_{s,i}/dx = n_{p,i} Nu \cdot 2\pi r_i \lambda (T - T_{s,i}), \quad i = 1, 2 \quad (5)$$

where C_s is the specific heat of particles, $\rho_{s,i} = n_{p,i} \rho_a 4\pi r_i^3 / 3$ is the bulk density of particles (mass of particles per unit volume), and ρ_a is the material density of aluminum.

In the present analysis, we are primarily concerned with fuel-lean mixtures. In a mono-dispersed aluminum particle-laden flow, the flame usually consists of three distinct zones: the preheat, flame, and post flame regimes [20]. In the preheat zone, the reaction rate is negligibly small. Particles are heated by the surrounding gas until their temperature reaches the ignition point. In the flame zone, particles are ignited and totally consumed. In dual-sized aluminum-particle/air suspensions, the flames have a complex multistage structure, mainly due to the disparities of the ignition temperature and burning time between particles with different sizes. Two possible scenarios exist, as illustrated in Fig. 3. In the overlapping flame configuration, the heat release from the combustion of small particles heats up and ignites

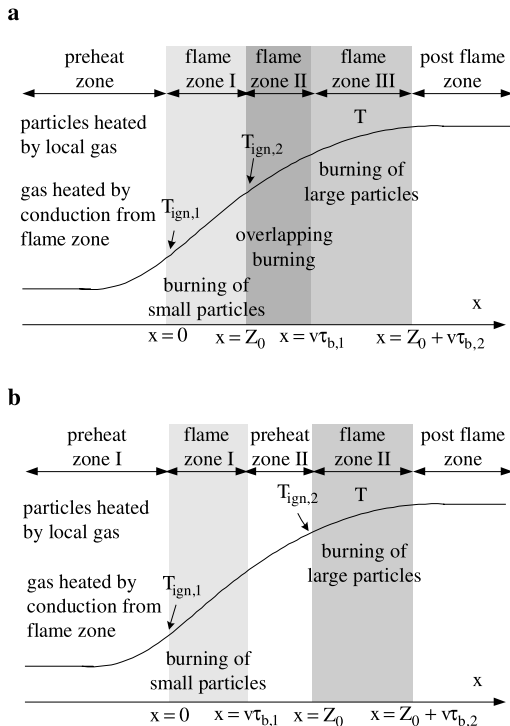


Fig. 3. Structures of bimodal-particle dust flames at fuel-lean conditions, (a) overlapping flame, and (b) separated flame.

large particles before complete burn-out of the former. Thus, the flame zones associated with the small and large particles overlap (Fig. 3a). In the separated flame configuration, the heat release from the burning of small powders is not sufficient to ignite large particles, and there exists two separated flame zones (Fig. 3b). Whether the flame exhibits an overlapping or a separated configuration depends on the mass concentration, particle size, ignition temperature, and burning time of each group of aluminum particles.

For fuel-lean mixtures, the burning time of a given particle group i is assumed to be equal to that of a single particle $\tau_{b,i}$. The overall burning rate of particle group i is thus considered constant with an averaged value, $B_{u,i}/\tau_{b,i}$, where $B_{u,i}$ is the initial mass concentration of particle group i . The heat-source terms in Eq. (2) can be written as

$$w_{F,i} Q = -B_{u,i} Q / \tau_{b,i}, \quad i = 1, 2 \quad (6)$$

By substituting Eqs. (6) and (1) into Eq. (2), the energy equation for the gas phase in the flame zone becomes

$$\rho_u S_L C_p dT/dx = \lambda d^2 T/dx^2 - \sum_{i=1}^2 B_{u,i} Q / \tau_{b,i} - \sum_{i=1}^2 n_{p,i} Nu 2\pi r_i \lambda (T - T_{s,i}) \quad (7)$$

The energy equation for the particle phase, Eq. (5), is not considered in the burning zones. It is only applied in the preheat regimes to solve for the temperatures of the gas phase at the ignition points of particles, which is prespecified as an input parameter. Because chemical reactions are neglected in the preheat zones, particle concentration remains unchanged, and the term in the parentheses on the left-hand side of Eq. (5) can be written as

$$\rho_{s,i} v C_s = \phi_i (m_F/m_o)_{st} \rho_u S_L C_s \approx (B_{u,i}/B_{st}) (m_F/m_o)_{st} \rho_u S_L C_s \quad (8)$$

Equation (5) thus takes the form

$$(B_{u,i}/B_{st}) (m_F/m_o)_{st} \rho_u S_L C_s dT_{s,i}/dx = n_{p,i} Nu 2\pi r_i \lambda (T - T_{s,i}) \quad (9)$$

To facilitate analysis, the temperatures and spatial coordinate are normalized as follows.

$$\theta = T/T_u, \quad \theta_{s,1} = T_{s,1}/T_u, \quad \theta_{s,2} = T_{s,2}/T_u, \quad y = x/(S_L \tau_{b,1}) \quad (10)$$

The location $y = 0$ is defined as the ignition point of small particles, and $y = Z = Z_0/(S_L \tau_{b,1})$ the ignition location of large particles. The parameter $P = \tau_{b,2}/\tau_{b,1}$, represents the ratio of the combustion times of large to small particles. Substituting the above parameters into Eqs. (7) and (9), we

obtain the following non-dimensional equations governing the temperature field in each regime,

$$d^2\theta/dy^2 - \kappa^2 d\theta/dy = \sum_{i=1}^2 \kappa^2 \eta_i (\theta - \theta_{s,i}) - \sum_{i=1}^2 \mu_i \kappa^2 (\theta_{ign,i} - 1) \quad (11)$$

$$d\theta_{s,i}/dy = (\theta - \theta_{s,i})/\xi_i, \quad i = 1, 2 \quad (12)$$

where $\theta_{ign,i}$ is the non-dimensional ignition temperature for particle group i , $\kappa = S_L/\sqrt{\tau_{b,1}\alpha}$ the non-dimensional flame speed, with $\alpha = \lambda/(C_p \rho_u)$ being the thermal diffusivity of the gas. The non-dimensional heat releases μ_i ($i = 1, 2$) can be determined from

$$\mu_1 = -B_{u,1} Q / (\rho_u C_p (T_{ign,1} - T_u)) \quad (13)$$

$$\mu_2 = -B_{u,2} Q / (\rho_u C_p (T_{ign,2} - T_u) P) \quad (14)$$

Finally, the non-dimensional thermal relaxation times of the particle and gas phases, ξ_i and η_i ($i = 1, 2$), are defined, respectively, as

$$\xi_1 = (m_F/m_o)_{st} r_1^2 \rho_a C_s / (3\alpha C_p \tau_{b,1} B_{st}) \quad (15)$$

$$\xi_2 = (m_F/m_o)_{st} r_2^2 \rho_a C_s P / (3\alpha C_p \tau_{b,2} B_{st}) \quad (16)$$

$$\eta_1 = 3B_{u,1} \tau_{b,1} \alpha / (r_1^2 \rho_a) \quad (17)$$

$$\eta_2 = 3B_{u,2} \tau_{b,2} \alpha / (r_2^2 \rho_a P) \quad (18)$$

By solving the energy conservation equation for each zone and matching the resultant temperature and heat flux at the interfacial boundaries, an algebraic equation for the flame speed can be obtained,

$$k_1 = \{ \mu_1 [1 - \exp(-\kappa^2)] + \mu_2 [1 - \exp(-\kappa^2 P)] \times \exp(-\kappa^2 Z) (\theta_{ign,2} - 1) / (\theta_{ign,1} - 1) \} / (1 + k_1 \xi_1) \quad (19)$$

where

$$k_1 = 0.5 \left\{ \kappa^2 - 1/\xi_1 + \sqrt{(\kappa^2 - 1/\xi_1)^2 + 4\kappa^2 (\eta_1 + 1/\xi_1)} \right\}$$

Equation (19) is general and valid for the both the overlapping and separated flame configurations. If μ_2 is set to 0 and the second group of particles are removed from the fuel formulation, the equation for a mono-dispersed mixture is recovered [20],

$$k_1 = \mu_1 [1 - \exp(-\kappa^2)] / (1 + k_1 \xi_1) \quad (20)$$

Equation (19) is supplemented by an expression relating the ignition temperature of large particles, $\theta_{ign,2}$, to its location Z ,

$$\theta_{ign,2} = f_i(\theta_{ign,1}, \kappa, \mu_1, \mu_2, \xi_1, \xi_2, \eta_1, \eta_2, Z, P), \quad i = 1, 2 \quad (21)$$

Note that the explicit forms of f_i (not shown here) are different for the overlapping and separated flame configurations. Equations (19) and (21) must be solved simultaneously for the flame speed S_L and the parameter Z , which falls in the range of $0 < Z < 1$ for an overlapping flame and $Z > 1$ for a separated flame.

4. Aluminum particle ignition temperature and burning time

The current analysis requires the particle ignition temperature, $T_{ign,i}$ and burning time, $\tau_{b,i}$, be specified as input parameters, both of which are a function of particle size. For large particles ($>100 \mu\text{m}$), most experimental studies [21,22] indicated that ignition is achieved at a temperature near the melting point of aluminum oxide (i.e., 2350 K). It was conjectured that the particle is covered by an impervious oxide shell, and aluminum does not ignite until the oxide shell melts or breaks up near its melting temperature under the effect of aluminum thermal expansion. For nano-sized particles, however, ignition has been observed to occur at temperatures as low as 900 K [9]. Recent studies [24] also indicate that aluminum particles with diameters of 1–100 μm could be ignited over a wide range of temperatures from 1000 to 2300 K. Trunov et al. [13] suggested that aluminum oxidation and polymorphic phase transformations of the alumina shell are responsible for these diverse ignition temperatures. They developed an ignition model based on such concepts and their results are adopted in the current analysis.

For micron and larger-sized particles, which usually burn under diffusion-controlled conditions, numerous data exists on their burning times. Several d^n -models, with n ranging from 1.5 to 2.0, have been proposed. In Ref. [23], almost 400 datum points for single particle burning times in various oxidizer environments were collected from over ten different sources. Correlations were established and the following particle burning-time model was proposed,

$$\tau_b = C_1 d^{1.8} / (T_0^{0.2} p^{0.1} X_{\text{eff}}) \quad (22)$$

where X_{eff} is the effective oxidizer mole fraction, $X_{\text{eff}} = C_{\text{O}_2} + 0.6C_{\text{H}_2\text{O}} + 0.22C_{\text{CO}_2}$, p the pressure in atmospheres, T_0 the initial temperature in Kelvin, d the particle diameter in μm , and C_1 a constant ($=0.00735$). This $d^{1.8}$ -law model is employed herein for micron and larger-sized particles.

Information about the burning time of nano-sized particles is limited, and no suitable model is currently available. Since nano particles usually

burn under kinetically controlled conditions, it is theoretically expected that a $d^{1.0}$ -model based on the dominant surface reaction rate may be more suitable for the particle burning time [11]. Recently, Parr et al. [9] examined the combustion characteristics of aluminum particles using a hydrogen–oxygen–argon burner. The particle size ranged from 24 nm to 30 μm in diameter. The particles ignited and burnt in the post-combustion gases of the burner flame. The flame temperature was controlled between 900 and 2400 K by varying the amount of argon. Figure 4 shows the measured particle burning time as a function of particle size at burner flame temperatures of 1500 and 2000 K. For nano-sized particles, a $d^{0.3}$ model is observed instead of a $d^{1.0}$ law. In the experiments of Parr et al. [9], agglomeration of small particles could occur, suggesting that the measured data might actually be the burning time of agglomerated particles with a larger size. In addition, it was found that the burning times of nano particles were strongly dependent on the burner flame temperature. For example, the burning times at 1500 K are much greater than these at 2000 K. In contrast, the burning time of a micron-sized particle is only a weak function of the environmental gas temperature, as suggested by Eq. (22). Micron-sized particles burn with a detached diffusion flame, whose temperature is predetermined by the vaporization–dissociation temperature of aluminum oxide [11]. The surrounding gas temperature thus exerts a limited influence on the particle burning time. For nano-sized particles, however, heterogeneous surface reactions, which heavily depend on the environmental temperature, play a very important role. Based on the above observations, a kinetically controlled burning time model was proposed as follows,

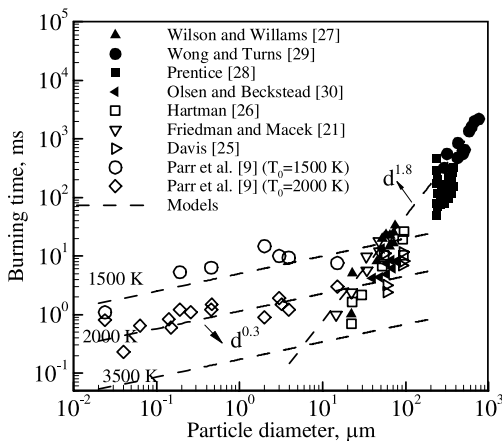


Fig. 4. Experimentally observed aluminum particle burning time as function of particle diameter. (see above-mentioned references for further information)

$$\tau_b = \frac{d^{0.3}}{C_2 e^{-E_b/RT} \cdot X_{\text{eff}}} \quad (23)$$

where d is in cm, $C_2 = 5.5 \times 10^4$, $E_b = 73.6$ kJ/mol, and R is universal gas constant. The model results are also shown in Fig. 4 for comparison. It was observed that the curve of the $d^{1.8}$ model for micron-particles intersects with that of the $d^{0.3}$ model for nano particles with a flame temperature of 2000 K at a particle diameter of 20 μm . The same curve intersects that of the $d^{0.3}$ model for nano particles at 3500 K at particle diameter of 6.0 μm . These results suggest that particles with diameters on the order of several micrometers could be in a transition region from diffusion- to kinetics-controlled combustion, where either model is applicable.

5. Results and discussions

The analytical model described in Section 3 is employed to analyze the flame characteristics of bimodal-particle laden flows. Particle diameters are 100 nm and 6.5 μm . The corresponding ignition temperatures are 1350 and 2100 K, respectively. For aluminum particles at both sizes, the estimated Stokes number St is much less than unity, confirming the validity of the assumption (3) adopted in the theoretical modeling. The $d^{0.3}$ and $d^{1.8}$ burning-rate laws are employed to determine burning times. Note that as a nano particle passes through the flame, its surrounding environmental temperature gradually increases. Thus, the burning rate of nano particles is taken from the data at a mean temperature around 2000 K. Figure 5 shows the predicted flame speed as a function of the nano-particle mass fraction in the fuel formulation, p_n , at the equivalence ratio $\phi = 0.85$. Also included in the figure is the experimental data for an equivalence ratio of

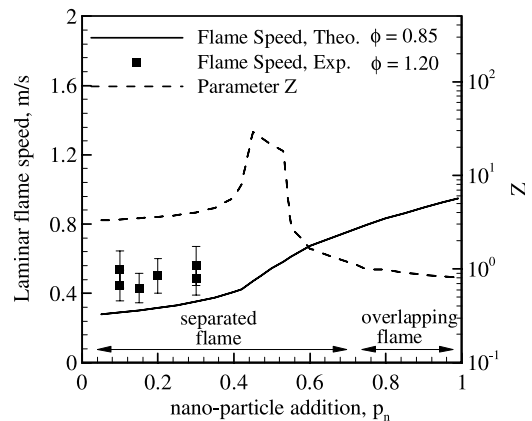


Fig. 5. Effect of mass percentage of nano particles in fuel formulation on flame speed.

1.2. The calculated flame speed increases with increasing nano-particle loading, p_n , a trend consistent with the experimental observation. For mixtures with $p_n < 75\%$, the flame displays a separated structure with $Z > 1$. This result explains the observed thicker flame zone of the bimodal mixture ($p_n = 20\%$) shown in Fig. 2. The distance between these two separated flame zones, Z , reaches a maximum at about $p_n = 40\%$. For mixtures with $p_n > 75\%$, overlapping flame structures were observed ($Z < 1$).

Figure 6 shows the temperature profiles for different values of p_n . It is obvious that a separated flame is much wider than an overlapping flame. For a separated flame with a small p_n , the combustion of micron-sized particles provides the majority of the heat release for heating and ignition of all the particles. With an increase in p_n , the heat release in the micron-sized particle flame zone decreases, and consequently the heating rate of micron-sized particles slows down and ignition is delayed. The flame zone of larger particles thus moves away from that of smaller particles (see the temperature profiles for $p_n = 10\%$, 30% , and 40%). As p_n further increases, the heat release from nano particles begins to play an important role in the heating and ignition processes. The flame zone of larger particles moves toward that of smaller particles (see the temperature profile for $p_n = 60\%$). For an overlapping flame with a large p_n , the combustion of nano particles produces a large amount of heat to ignite the micron-size particles, and soon increases the gas temperature above 3000 K. The larger-sized particles continue to burn and gradually increase the gas temperature to its maximum value around 3500 K (see the temperature profiles for $p_n = 80\%$ and 95%).

Figure 7 shows the predicted flame speed as a function of equivalence ratio for various p_n .

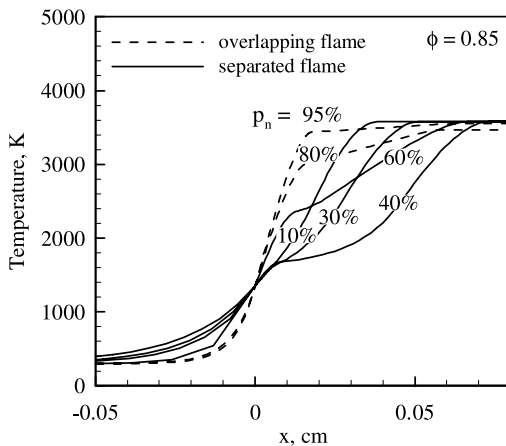


Fig. 6. Temperature profiles with different mass fractions of nano particles in fuel formulation, $\phi = 0.85$.

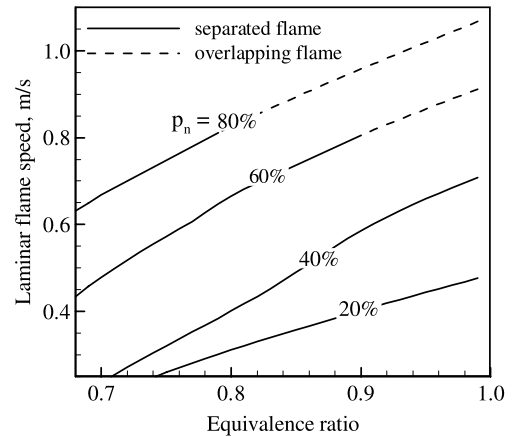


Fig. 7. Flame speed as function of equivalence ratio at different nano-particle mass fractions in fuel formulation.

The flame speed increases with increasing equivalence ratio. At a higher value of p_n , the flame displays a separated structure for very lean mixtures, and exhibits an overlapping configuration for near stoichiometric mixtures. At a lower value of p_n , however, the flame remains as a separated configuration for all mixtures at lean and near-stoichiometric conditions.

6. Conclusions

The combustion of bimodal nano/micron-sized aluminum particles with air was studied theoretically and experimentally in a well-characterized laminar particle laden flow. Experimentally, a Bunsen-burner type apparatus was constructed to investigate the flame characteristics of bimodal particles/air mixtures. The flame speed is positively affected by increasing the mass fraction of nano particles in the fuel formulation despite the lower flame luminosity and thicker flame zone. Theoretically, the overall fuel lean flames were assumed to consist of several different regimes, including the preheat, flame, and post flame zones. An analytical model for the flame speed and temperature distribution was established by solving the energy equation in each regime and matching the temperature and heat flux at the interfacial boundaries. Recent research results on the ignition temperatures and burning rates of nano particles were incorporated into the analysis. Reasonable agreement between theoretical results and experimental data was obtained in terms of the flame speed. At a low percentage of nano particles, the predicted temperature profile exhibited a separated flame structure. The phenomenon is consistent with the experimental observation of a thicker flame zone with two different burning regimes

associated with small and large particles. At a high percentage of nano particles, an overlapping flame configuration was observed.

Acknowledgments

This work was sponsored by the Office of Naval Research (ONR) under Grant No. N00014-03-1-0595. The support and encouragement provided by Dr. Gabriel Roy are gratefully acknowledged.

References

- [1] E.W. Price, R.K. Sigman, in: V. Yang, T.B. Brill, W.Z. Ren (Eds.), *Progress in Astronautics and Aeronautics*, AIAA, vol. 185, 2000, 663–687.
- [2] V.A. Babuk, V.A. Vassiliev, V.V. Sviridov, in: V. Yang, T.B. Brill, W.Z. Ren (Eds.), *Progress in Astronautics and Aeronautics*, AIAA, vol. 185, 2000, 663–687.
- [3] P. Bucher, L. Ernst, F.L. Dryer, R.A. Yetter, T.P. Parr, D.M. Hanson-Parr, in: V. Yang, T.B. Brill, W.Z. Ren (Eds.), *Progress in Astronautics and Aeronautics*, AIAA, vol. 185, 2000, 689–722.
- [4] K.P. Brooks, M.W. Beckstead, *Journal of Propulsion and Power* 11 (4) (1995) 769–780.
- [5] E.L. Dreizin, *Combust. Flame* 105 (1996) 541–556.
- [6] P. Bucher, R.A. Yetter, F.L. Dryer, E.P. Vicenzi, T.P. Parr, D.M. Hanson-Parr, *Combust. Flame* 117 (1999) 351–361.
- [7] P.E. DesJardin, J.D. Felske, M.D. Carrara, *Journal of Propulsion and Power* 21 (3) (2005) 478–485.
- [8] Y.S. Kwon, A.A. Gromov, A.P. Ilyin, E.M. Popenko, G.H. Rim, *Combust. Flame* 133 (2003) 385–391.
- [9] T.P. Parr, C. Johnson, D. Hanson-Parr, K. Higa, K. Wilson, *39th JANNAF Combustion Subcommittee Meeting*, December 2003.
- [10] S. Alavi, D.L. Thompson, *Journal of Physical Chemistry A* 110 (2006) 1518–1523.
- [11] R.A. Yetter, F.L. Dryer, *Micro-Gravity Combustion: Fire in Free Fall*, Academic Press, 2001, pp. 419–478.
- [12] K. Park, D. Lee, A. Rai, D. Mukherjee, M.R. Zachariah, *Journal of Physical Chemistry B* 109 (2005) 7290–7299.
- [13] M.A. Trunov, M. Schoenitz, E.L. Dreizin, *Combustion Theory and Modeling* 10 (4) (2006) 603–623.
- [14] S. Goroshin, M. Bidabadi, J.H.S. Lee, *Combust. Flame* 105 (1996) 147–160.
- [15] S. Goroshin, I. Fomenko, J.H.S. Lee, *Proc. Combust. Inst.* 26 (1996) 1961–1967.
- [16] Y. Shoshin, E.L. Dreizin, *AIAA Journal* 42 (7) (2004) 1416–1426.
- [17] G.A. Risha, Y. Huang, R.A. Yetter, V. Yang, *AIAA Paper*, AIAA-2005-0739, 2005.
- [18] S. Goroshin, M. Kolbe, J.H.S. Lee, *Proc. Combust. Inst.* 28 (2000) 2811–2817.
- [19] G. Joulin, *Proc. Combust. Inst.* 18 (1980) 1395–1403.
- [20] Y. Huang, G.A. Risha, V. Yang, R.A. Yetter, *AIAA Paper*, AIAA 2005-0738, 2005.
- [21] R. Fridman, A. Macek, *Combust. Flame* 6 (1962) 9–19.
- [22] Y. Zhu, Y. Yuasa, *Combust. Flame* 115 (1998) 327–334.
- [23] M.W. Beckstead, *Combustion, Explosion, and Shock Waves* 41 (5) (2005) 533–546.
- [24] M.A. Trunov, M. Schoenitz, F.L. Dreizin, *Propellants, Explosives, Pyrotechnics* 30 (1) (2005) 36–42.
- [25] A. Davis, *Combust. Flame* 7 (4) (1963) 359–367.
- [26] K.O. Hartman, in: *Proceedings of 8th JANNAF Combustion Meeting*, vol. 1, 1971, pp. 1–24.
- [27] R.P. Wilson, F.A. Williams, *Proc. Combust. Inst.* 13 (1971) 833–845.
- [28] J.L. Prentice, *AIAA Paper*, AIAA-1974-146, 1974.
- [29] S.C. Wong, S.R. Turns, *Combustion Science and Technology* 52 (1987) 221–242.
- [30] S.E. Olsen, M.W. Beckstead, *Journal of Propulsion and Power* 12 (4) (1996) 662–671.

Comment

Samuel Goroshin, McGill University, Canada. The results presented here are based on a model [1] that requires input of external parameters such as ignition temperatures and combustion times for both particle sizes. As you correctly stated, it is most likely that nano-sized particles react in the flame in the kinetic regime. However, kinetically reacting particles do not have an ignition temperature. Particle ignition actually means transition to the diffusion combustion regime and therefore is not defined for a kinetically controlled particle. What is more, the combustion time for kinetically reacting particles also cannot be treated as an external parameter and is an eigenvalue of the problem together with the flame speed and the flame temperature profile. Thus, it seems that this model is not adequate for kinetically reacting particles.

It is most likely that a considerable fraction, if not all, of the nano-sized powder is dispersed in the form of agglomerates. Agglomerates can also form in the flow after dispersion. Have you performed any experimental measurements that allow estimation of the agglomerated mass fraction and the size of agglomerates?

Reference

- [1] S. Goroshin, M. Kolbe, J.H.S. Lee, *Proc. Combust. Inst.* 28 (2000) 2811.

Reply. Following common practice, the ignition temperature is defined as the temperature at which the particle rapidly heats up and undergoes vigorous exothermic reactions. For micron- and larger-sized alumi-

num particles, such a temperature usually corresponds to the melting point of aluminum oxide (i.e., 2350 K). For nano-sized particles, ignition has been observed to occur at temperatures as low as 900 K ([9] in paper), due to high specific area and phase transformations of the surface layer. We disagree on the notion that kinetically reactive particles such as nano particles do not have an ignition temperature.

We appreciate the comment that the combustion time for nano particles, in a strict sense, cannot be pre-specified as it is a function of particle diameter and temperature (Eq. 23). To address this issue, a more complete analysis has been conducted taking into account the variations of ambient temperature and particle size. For a separated flame with a low loading density of nano-sized particles, the calculated flame speed and spatial structure appears to be insensitive to the environmental temperature. For an overlapped flame with a high loading density of nano-sized particles, the qualitative trend of the flame behavior remains identical to that predicted

by the present analysis, although the quantitative values change modestly. Thus, we feel that the current model based on a simplified assumption is valid and capable of capturing the main features of bimodal particle dust combustion. The reasonable agreement between experimental data and model predictions further supports this conclusion.

It is likely that particles may agglomerate in the flow path, and thus special attention was given to preventing particle agglomeration in the experiments. The burner was carefully designed to provide high-intensity, fine-scale turbulence throughout the entire mixer, and to minimize stagnation regions if there are any. Regions with high shear flows in which particles may coalesce were also avoided. In spite of those efforts to maximize particle dispersion, no measurement was conducted to assess the degree of particle agglomeration in the flowfield due to obstacles in performing diagnostics at nano scales. This issue should be addressed in the future.